sustainability

MDPI

Article

Study on Excavation Damage Characteristics of Surrounding Rock in Deeply Buried Tunnels by Particle Flow Code Simulation

Yanbin Zhang [1,*], Huazhong Yu [1,*], Huanchun Zhu [2] and Yongsheng Zhu [3]

[1] Safety Technology Training Institute, Henan Polytechnic University, Jiaozuo 454000, China
[2] Itasca Consulting China, Ltd., Wuhan 430205, China
[3] HydroChina-ITASCA R&D Center, Hangzhou 310014, China
* Correspondence: yanbin303@163.com (Y.Z.); yhz@hpu.edu.cn (H.Y.)

Abstract: This study is aimed at investigating the excavation damage characteristics of surrounding rock in Jinping deeply buried marble tunnels, China. According to the acoustic detection results of tunnel cross-sections under the condition of tunnel boring machine (TBM) obtained on site, the PFC microscopic parameters of Types II/III tunnel marble were simulated and calibrated through the PFC^{2D} program. In doing so, the excavation damage characteristics of surrounding rock of deeply-buried sections in Jinping diversion tunnels were simulated. The results reveal that the excavation damage zones (EDZ) of surrounding rock of Types II/III marble sections in Jinping tunnels are unevenly distributed around the tunnels; the largest zone is located from the top arch to the north arch shoulder. The EDZ depth and damage degree of surrounding rock rise with the increase in buried depth, and they also increase with the decrease in rock quality. Generally, the maximum damage depth of Type III surrounding rock is about 1.0 m larger than that of Type II surrounding rock under the same buried depth, which is basically consistent with the detection results of the relaxation depth of surrounding rock. The simulation well discloses the excavation damage characteristics of surrounding rock in Jinping deeply buried tunnels.

Keywords: deeply buried tunnel; excavation damage; damage evolution; particle flow code; acoustic detection results; TBM excavation

check for updates

Citation: Zhang, Y.; Yu, H.; Zhu, H.; Zhu, Y. Study on Excavation Damage Characteristics of Surrounding Rock in Deeply Buried Tunnels by Particle Flow Code Simulation. *Sustainability* **2022**, *14*, 16632. https://doi.org/10.3390/su142416632

Academic Editors: Ping Chang, Danqi Li, Saisai Wu, Jianhang Chen and Jianjun Ma

Received: 1 September 2022
Accepted: 7 December 2022
Published: 12 December 2022

Publisher's Note: MDPI stays neutral with regard to jurisdictional claims in published maps and institutional affiliations.

Copyright: © 2022 by the authors. Licensee MDPI, Basel, Switzerland. This article is an open access article distributed under the terms and conditions of the Creative Commons Attribution (CC BY) license (https://creativecommons.org/licenses/by/4.0/).

1. Introduction

As rock mass is in a complex three-dimensional stress state in the natural environment, the excavation-induced pressure relief will lead to stress redistribution of surrounding rock near the excavation face. During stress adjustment, the secondary stress will cause fracturing damage of surrounding rock and formation of excavation damage zones (EDZ), when it reaches a certain extent [1]. Bäckblom and Martin [2] held that the surrounding rock EDZ was formed by the yielding and outward development of rock mass or local rock mass near the excavation face. Read [3] further explored the causes of EDZ formation in surrounding rock and thought that the tensile stress zone in tunnel surrounding rock may also be one of the causes of surrounding rock excavation damage during rock excavation. In engineering practice, the physical and mechanical properties of surrounding rock EDZ, the detection of EDZ range and the evaluation of damage degree are crucial to the stability of rock engineering structure and the optimization of support parameters [4–7].

Since the 1980s, for the purpose of safe storage of radioactive nuclear waste, European countries and the United States have successively established underground rock engineering test sites to study the fracturing damage characteristics of rock mass, including Underground Research Laboratory (URL) of AECL (Atomic Energy of Canada Limited) [8–11]; SKB Company and Aspö Hard Rock Laboratory (HRL) of Sweden [12] and Yucca Mountain test site of the United States [13]. They have carried out massive on-site tests, monitoring and testing work, and conducted in-depth research on the surrounding

rock EDZ. Among them, the research at URL is the most representative. According to a series of laboratory and on-site tests, monitoring and test research on Lac du Bonnet granite at URL, surrounding rock excavation damage is defined as an irrecoverable damage caused by excavation, including damages caused by impacts resulting from excavation methods (such as blasting energy release) and damages caused by crack propagation resulting from stress redistribution and environmental variations (such as temperature and humidity variations).

As the construction of deep rock engineering in China began, research were gradually conducted on surrounding rock excavation damage and some research results have been obtained [14–16]. For the purpose of analyzing the formation and evolution mechanism of EDZ, Yan et al. [17] comparatively analyzed the characteristics and causes of surrounding rock EDZ under two different excavation methods, namely Tunnel Boring Machine (TBM) and drilling and blasting, through an in situ test. Zhu et al. [18] monitored excavation deformation of underground powerhouse chamber of Dagangshan hydropower station for a long time, and concluded the distribution range and damage deterioration characteristics of underground chamber EDZ. Liu et al. [19] explored the localization characteristics and degree variations of surrounding rock excavation damage during TBM tunneling through an in situ acoustic emission monitoring test and particle flow code (PFC) numerical simulation.

Excavation damage will result in some permanent variations in the mechanical and hydraulic properties of surrounding rock, including a decrease in rock quality, a reduction of acoustic velocity, an increase in permeability, etc. These variations can be quantitatively tested through technical means such as acoustic detection, micro-seismic or acoustic emission detection, and permeability test. Among them, acoustic detection is widely used on engineering sites for its simple operation, high accuracy, and easy reading of results [20–22].

Due to the complexity of surrounding rock excavation damage mechanism, the calculation and theoretical analysis, especially numerical research, on the range of EDZ are not mature enough yet at present. It is difficult to accurately describe the non-linear behavior of rock mass and the excavation damage characteristics of surrounding rock based on the calculation method of continuum mechanics. The PFC is based on the discrete element method. This method starts from the state of contact between particles and its evolution characteristics to describe the basic mechanical properties of rock mass medium, and can reflect surrounding rock excavation damage and its variation characteristics caused by the development of rock micro-fractures [23–25]. Therefore, this method is quite suitable for studying the complex macro-meso mechanical behavior of rock mass medium.

In this study, first, the description method of surrounding rock EDZ for the fracturing damage behavior of surrounding rock after excavation of Jinping deeply buried marble tunnels was selected based on the analysis on surrounding rock excavation damage and its evolution characteristics. Second, according to the acoustic detection results of cross-sections in shallow marble tunnel sections under TBM conditions, PFC microscopic parameters of Types II/III marble sections in Jinping tunnels were simulated and calibrated by the PFC^{2D} program. Finally, surrounding rock excavation damage characteristics of the deep tunnel sections of Jinping Types II/III marble tunnels under TBM conditions were simulated with the aid of microscopic parameters of the PFC model of deeply buried marble. This research provides reference for surrounding rock stability analysis and support optimization design in deep tunnel sections.

2. Surrounding Rock Excavation Damage and Its Numerical Description

2.1. ED and its Evolution Characteristics

Research on surrounding rock excavation damage are mostly focused on the variations of mechanical properties and state of surrounding rock caused by stress redistribution without considering the effect of external factors such as blasting.

In engineering practice of deeply buried rock mass, surrounding rock excavation damage directly reflects the surrounding rock excavation response under the condition of deeply buried high stress. Therefore, for the purpose of grasping the excavation damage

process of tunnel surrounding rock, it is necessary to study the variations of rock excavation response of tunnel surrounding rock at different locations under excavation. Figure 1 shows the research understanding of the mechanism and variations of surrounding rock excavation damage in a mass mining technology (MMT) project [26] during tunnel excavation in deeply buried mines. It directly describes the sub-zones and variation mechanism of tunnel surrounding rock excavation damage (the red lines represent visible or invisible damage cracks). The left diagram in Figure 1 exhibits four sub-zones (namely, elastic zone, micro-seismic zone, yield zone and excavation zone) of surrounding rock divided according to the state of surrounding rock under the high stress condition of the MMT project. The right schematic diagram in Figure 1 shows the stress paths experienced by surrounding rock in different sub-zones in the past and the possible evolution trends in the future, which are briefly described as follows.

1. Elastic zone: i.e., linear elastic response zone, which corresponds to the transition stage from the self-stress concentration zone of surrounding rock to the original rock stress zone. There is no stress damage in surrounding rock. In the spatial diagram of stress path (right diagram of Figure 1), the stress path has not reached the crack initiation strength envelope and is still in the A-B section.
2. Micro-seismic zone: i.e., the stress concentration zone, in which a series of micro-seismic events may occur along with the stress concentration process of surrounding rock. The stable development of internal damage of surrounding rock falls into a discontinuous stage. The division of this zone is based on the fact that the stress level exceeds the crack initiation strength of rock mass, resulting in the dislocation deformation of new and old cracks in rock mass, which is caused by the accumulation of internal damage in rock mass and the propagation of cracks along the tip of structural plane. This stage emphasizes the development process of damage, which corresponds to the B-C section of the spatial schematic diagram of stress path in the right diagram of Figure 1.
3. Yield zone: corresponding to the post-peak deformation stage of rock mass, which is the final result of damage crack accumulation, propagation, and stress level reaching its strength limit and forming macroscopic failure zones. This zone also falls into a yield zone and a failure zone. For brittle rock mass, these two differ in failure forms in reality. For example, whether stress-type failure, such as rib falling and spalling, has occurred. This zone corresponds to the C-D section of the spatial schematic diagram of stress paths in Figure 1.
4. Excavation zone: i.e., the rock mass that is excavated manually.

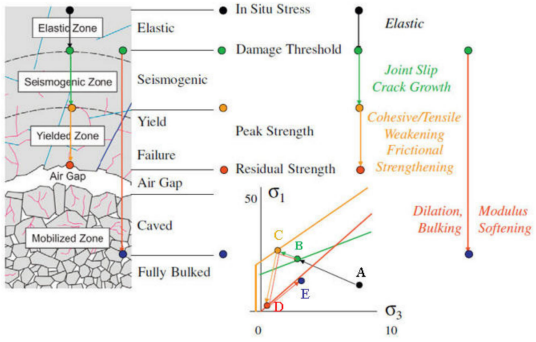


Figure 1. Evolution mechanism of excavation damage of surrounding rock [26,27].

Elastic zone, micro-seismic zone and yield zone constitute the possible existence forms of surrounding rock in the damage evolution process with the variation of stress level. However, under the driving action of stress, surrounding rock tends to vary from the current state to the next state. For example, a universal variation process of elastic zone to micro-seismic zone to yield zone, and this variation process is irreversible, which is the essence of the influence of excavation damage on the state of surrounding rock.

The influence of excavation damage on the state of surrounding rock finally results in the variation of rock properties. That is, the damage evolution reflects the weakening process of surrounding rock, which is reflected in the loss of rock strength and the variation of physical properties of surrounding rock after the variation of internal structural characteristics of rock, such as the degradation of deformation modulus. The influence of excavation damage on the deformation characteristics of rock mass depends on the stress level and the mechanical properties of surrounding rock. A higher stress level leads to a severer excavation damage. The mechanical properties of surrounding rock determine the influence of excavation damage on the deformation characteristics of rock mass from another aspect. This is because the mechanical properties of surrounding rock largely influence the crack type, i.e., the ratio of tensile cracks to shear cracks in damaged rock mass.

2.2. Numerical Description of EDZ

From the perspective of exploring surrounding rock excavation damage, the failure of surrounding rock and even the failure of V-shaped rib falling are considered as the results of damage evolution. Based on the understanding of existing research results, when the stress level of surrounding rock reaches the peak strength and evolves into the residual strength, the damage of surrounding rock is uneven, and the damage range may also contain relatively complete rock blocks, that is, the damage range includes the localization of damage, which is proven by a large number of on-site practices [28–30].

The localization of surrounding rock excavation damage is caused by the development, propagation, intersection, and connection of micro-cracks, which then leads to the local adjustment of surrounding rock stress. It is difficult to microscopically describe the surrounding rock EDZ through continuous mechanical method (CMM). As shown in Figure 2, the loose zones or yield zones of surrounding rock obtained by the commonly used CMM are often evenly distributed around the hole. That is, once a unit is yielding, the mechanical properties of the unit will not vary through CMM. Unlike CMM, the PFC based on discontinuous mechanical method (DMM) can reflect the uneven distribution characteristics of rock mass and micro-fracture strength, thus reflecting the localization of excavation damage. The enlarged figure on the right of Figure 2 displays the damage and load distribution of the tunnel vault. Obviously, the damage can be locally distributed at a certain depth, and its surrounding area is still relatively complete and bears a certain load. The right diagram in Figure 2 also reveals an important characteristic: When the crack develops to a certain extent (such as the shallow tens of centimeters), surrounding rock loses its bearing capacity, and the calculation results show an almost zero contact force between particles, which corresponds to the shallow fracturing zone of surrounding rock at the site. Yet the deeper part of surrounding rock corresponds to the EDZ. They are well consistent with the observation results of the fracturing zone, the test results of the EDZ and the results in Figure 1 of the tunnel surrounding rock in Jinping engineering site, which confirms the effectiveness of the DMM-based PFC in terms of basic principle and engineering practice.

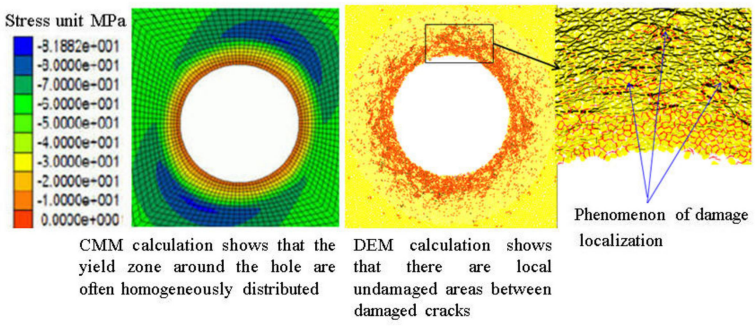


Figure 2. Differences between two mechanical methods (DMM and CMM) in description of the excavation damage zone of the surrounding rock.

From the perspective of on-site actual situation, as the buried depth increases, overall, the damage degree of surrounding rock shows an increasing trend; and the development time from damage to macro fracturing is shortened accordingly. In general, the increase in buried depth influences excavation damage mainly from two aspects, namely an increase in damage depth and a rise of damage degree. The former can be reflected through both CMM and DMM, but the latter is difficult to describe through CMM. Figure 3 shows the calculation results of tunnel EDZ with the aid of the DMM-based FLAC program (a) and the CMM-based PFC program (b), respectively.

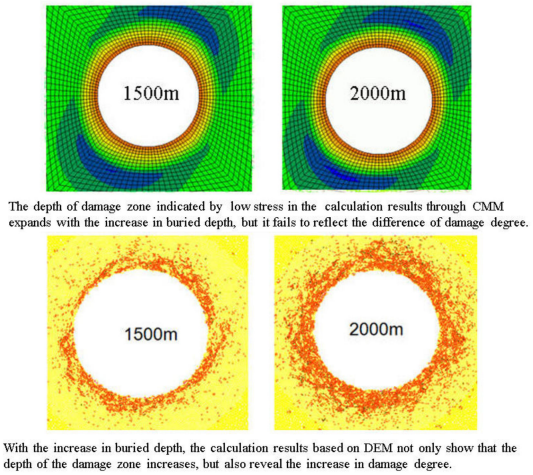


Figure 3. Influence of buried depth changes on damage distribution described by two mechanical methods(DMM and CMM).

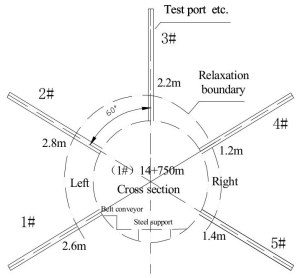
It can be seen from Figure 3 that the low-stress zone of surrounding rock in the calculation results through CMM mainly reflects the yield result of surrounding rock. The range of the low-stress zone expands with the increase in buried depth, but the stress level coincides with the residual strength of surrounding rock, and does not vary with the variation of buried depth. Therefore, it fails to reflect the difference of damage degree. With the increase in buried depth, the PFC calculation results based on DMM not only show the increase in excavation damage depth, but also reveal the rise of EDZ crack density, i.e., the increase in damage degree.

CMM has inevitable defects in describing mechanical problems of marble rock mass, such as the fracturing damage. In contrast, the DMM-based PFC program, which reflects its macroscopic mechanical behavior from the perspective of microscopic mechanics of medium, can achieve the following goals: First it can reasonably describe the important mechanical indicators such as crack initiation strength, peak strength and residual strength of rock mass; second, it can reflect the degradation of surrounding rock deformation modulus caused by excavation damage; third, it can reflect important surrounding rock excavation response characteristics [31,32], such as the increase in damage localization and damage degree with the increase in buried depth. Considering the rationality of damage research method, the DMM-based PFC program is obviously superior in the study on the excavation damage problem of Jinping deep tunnels.

3. On-Site Test Results of Excavation Damage Depth

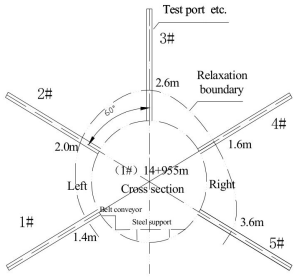
Acoustic emission monitoring during excavation is the best method to identify the excavation damage depth of surrounding rock, but it is not systematically conducted on site. Therefore, determination of the excavation damage depth of surrounding rock mainly depends on the on-site acoustic detection results.

Figure 4 shows the acoustic detection results of partial cross-sections of Jinping 1# and 3# diversion tunnels. The acoustic detection results of the above tunnel cross-sections were summarized and counted (Table 1).



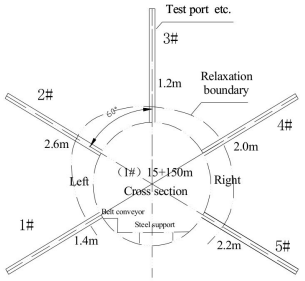
Detection cross-section in Type II surrounding rock

Detection hole No.	1#	2#	3#	4#	5#
Relaxation depth（m）	2.6	2.8	2.2	1.2	1.4



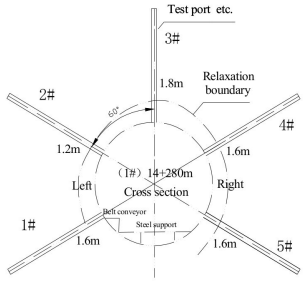
Detection cross-section in Type II surrounding rock

Detection hole No.	1#	2#	3#	4#	5#
Relaxation depth（m）	1.4	2.0	2.6	1.6	3.6



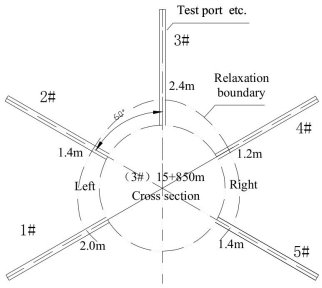
Detection cross-section in Type II surrounding rock

Detection hole No.	1#	2#	3#	4#	5#
Relaxation depth（m）	1.4	2.6	1.2	2.0	2.2



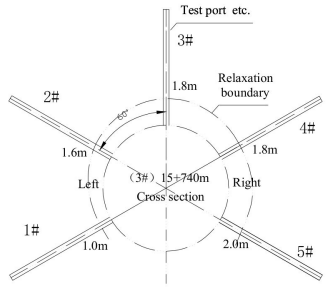
Detection cross-section in Type II surrounding rock

Detection hole No.	1#	2#	3#	4#	5#
Relaxation depth（m）	1.6	1.2	1.8	1.6	1.6



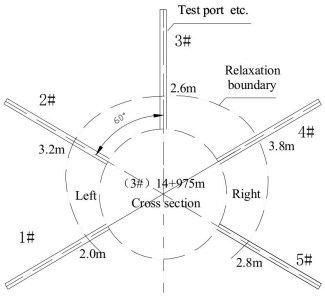
Detection cross-section in Type II surrounding rock

Detection hole No.	1#	2#	3#	4#	5#
Relaxation depth（m）	2.0	1.4	2.4	1.2	1.4



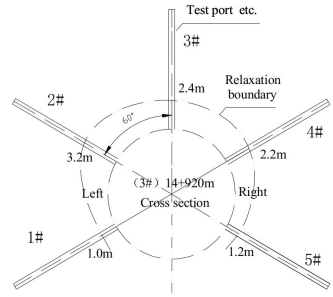
Detection cross-section in Type II surrounding rock

Detection hole No.	1#	2#	3#	4#	5#
Relaxation depth（m）	1.0	1.6	1.8	1.8	2.0



Detection cross-section in Type II surrounding rock

Detection hole No.	1#	2#	3#	4#	5#
Relaxation depth（m）	2.0	3.2	2.6	3.8	2.8



Detection cross-section in Type II surrounding rock

Detection hole No.	1#	2#	3#	4#	5#
Relaxation depth（m）	1.0	3.2	2.4	2.2	1.2

Figure 4. Schematic diagram of sonic detection results of some cross sections of Jinping 1#, 3# diversion tunnels (left-north, right-south).

Table 1. Statistics table of sonic detection results of cross sections of Jinping 1#, 3# diversion tunnels excavated by TBM (Unit:m).

Detection Pile No.	Depth	Strata Lithology	Rock Type	North Wall	North Arch Shoulder	Top Arch	South Arch Shoulder	South Wall	Remark
(1#)15+150	1427	T_{2y}^{4}	III	2.6	2.8	2.2	1.2	1.4	/
(1#)14+955	1517	T_{2y}^{5}	III	1.4	2.0	2.6	1.6	3.6	/
(1#)14+750	1536	T_{2y}^{5}	II	1.4	2.6	1.2	2.0	2.2	/
(1#)14+280	1694	T_{2y}^{6}	II	1.6	1.2	1.8	1.4	1.6	1.6
(1#)12+970	1644	T_{2y}^{5}	II	1.2	1.2	1.2	1.0	0.8	/
(3#)15+850	935	T_{2y}^{6}	II	2.0	1.4	2.4	1.2	1.4	/
(3#)15+740	1028	T_{2y}^{5}	IIb	1.0	1.6	2.4	1.8	1.0	/
(3#)15+250	1293	T_{2y}^{5}	II	1.8	1.8	1.8	1.0	2.0	/
(3#)15+200	1319	T_{2y}^{5}	III	1.0	3.4	3.4	3.2	1.2	/
(3#)14+975	1418	T_{2y}^{5}	III	2.0	3.2	2.6	3.8	2.8	/
(3#)14+920	1430	T_{2y}^{5}	III	1.0	3.2	2.4	2.2	1.2	/
(3#)14+635	1573	T_{2y}^{5}	III	1.4	2.6	2.6	3.0	3.4	/
(3#)14+505	1636	T_{2y}^{5}	III	2.6	2.6	2.4	2.2	1.4	/
(3#)12+850	1724	T_{2y}^{5}	II	1.4	1.8	1.6	2.4	1.2	/

It can be known from Figure 4 and Table 1 that in the statistical results of Type II surrounding rock, the depth of low-wave velocity zone revealed by acoustic detection results generally displays a relatively even distribution on the cross-sections; only the depth near the top arch is relatively large, which is basically consistent with the ground stress state along the Jinping diversion tunnels. The depth of low-wave velocity zone indicated by the acoustic detection results of Type III surrounding rock cross-sections in the top arch zone is generally larger when compared with the detection results of Type II surrounding rock cross-sections.

Since the on-site acoustic detection results do not illustrate the specific geological conditions corresponding to the boreholes, especially for the joint development characteristics in the boreholes, it is difficult to reasonably determine the depth of the EDZ according to the detection results. The reason is that the depth of the low-wave velocity zone of surrounding rock in the tunnel cross-sections is mainly affected by two factors, i.e., the yield degree of surrounding rock and the influence of the structural plane. Relevant research results disclose that the existence of the structural plane can lead to surrounding rock excavation damage in a wider depth range near it, and thus affects the distribution characteristics of low-wave velocity zones on the cross-sections. In the ideal condition without the influence of the structural plane, the shape of the low-wave velocity zone on the tunnel cross-sections is mainly influenced by the initial stress state of the cross-sections, which is the severest in the north arch shoulder and south arch foot of Jinping tunnels. This prediction result is not completely consistent with the acoustic detection results, indicating that the structural plane may exert a significant impact on the test results of low-wave velocity zone of surrounding rock. On Jinping tunnel engineering site, except for the plane, the dominant structural plane in tunnel surrounding rock is NWW and NE joints, in which the NWW joints are developed the most. Among the three groups of structural planes, the angle between the NWW joints and the tunnel axis is the smallest. Therefore, when a steeply dipping NWW joint appears in the top arch zone, it is difficult to be exposed by the test holes arranged vertically, which basically does not affect the fracturing damage of surrounding rock in the top arch zone. However, the intersection angle between NWW joints and acoustic holes in places except the top arch is large, so it is more likely to affect the acoustic detection results.

Figure 4 shows the acoustic detection results of partial cross-sections of Jinping 1# and 3# diversion tunnels. It can be seen from Figure 4 that the on-site acoustic detection results of the tunnel cross-sections do not reveal a clear correlation between the depth of the low-wave velocity zone of surrounding rock and the depth of the tunnels. However, this

does not violate the basic law that the depth of the low-wave velocity zone of surrounding rock rises with the increase in the depth of the tunnels under the same conditions. The reasons are as follows: (1) The distribution of the ground stress along the tunnel axis does not completely correspond to the depth of the tunnels, and local geo-stress fields exist in the folds along the tunnels. (2) Rock quality exerts a significant impact on the depth of low-wave velocity zone of surrounding rock. The variation of rock quality along the tunnels may cover up the relationship between the depth of low-wave velocity zone and the buried depth.

Table 1 shows that in the acoustic detection results of relaxation depth of tunnel cross-sections, the relaxation depth of cross-sections corresponds to a large discreteness, and even the detection results of different test holes in the same cross-section may differ much due to the difference in rock quality between cross-sections and the influence of structural plane and local stress field. In the above test results, it can be considered that when the test results of different test holes under similar conditions differ much, a smaller depth of low-wave velocity zone can better represent the EDZ distribution of surrounding rock under "general conditions". When the depth of low-wave velocity zone jumps, it is likely to be related to specific structural planes and cannot represent general conditions. Hence, when the excavation damage depth of surrounding rock of the deeply buried tunnel sections is predicted by the numerical method based on the above results, the acoustic detection results of the relaxation depth of the cross-sections in Table 1 need to be "generalized". If the structural plane in the rock mass is homogenized, that is, the influence of the structural plane is reflected in the integrity index of the rock mass, and the corresponding realistic conditions are "general conditions", which means that the "homogenized" calculation results of the model should be consistent with the on-site test results under "general conditions".

4. Parameter Calibration of Jinping Types II/III Marble

Zhang et al. [33] conducted laboratory triaxial compression tests and found that the post-peak deformation and failure of Jinping marble corresponded to notable brittle-ductile-plastic transformation characteristics with the increase in confining pressure. Fairhurst [34] revealed such important characteristics in the laboratory tests of Tennesse marble. That is, marble was brittle under low confining pressure, plastic under high confining pressure, and corresponded to brittle-extension or extension-plastic transformation under middle confining pressure. Yu et al. [35] conducted research and found that the brittle-ductile-plastic transformation characteristics of marble were closely related to the internal tension of medium and the development degree of shear cracks. The complex post-peak mechanical behavior of marble reflected the extreme complexity of its internal deformation and failure mechanism [36].

When the fracturing damage depth of surrounding rock excavated by TBM in Jinping deeply-buried tunnels was predicted through particle flow method, the parameters were calibrated as follows. First, compressive strength tests were conducted on Jinping Types II/III marble PFC model specimens under confining pressure. In doing so, the macroscopic mechanical properties of the model specimens and the peak strength envelope of the specimen under different confining pressures complied with the description of Types II/III marbles by the Hoek–Brown failure criterion; and the brittle-ductile-plastic transformation characteristics of the model specimen were naturally reflected in the compression test. Then, the excavated tunnel section of Jinping Types II/III marble was numerically simulated based on the preliminarily obtained PFC microscopic parameters of marble. Moreover, the consistency between the calculation results and the measured results was examined, and the parameters were further debugged. Ultimately, the fracturing damage depth of surrounding rock after tunnel excavation was consistent with the acoustic detection results of the relaxation depth of surrounding rock on site. At this time, the PFC model medium satisfied the description of Types II/III marble by the Hoek–Brown failure criterion and the acoustic detection results of the relaxation depth of surrounding rock, and naturally

reflected the brittle-ductile-plastic transformation characteristics. It can be held that the PFC microscopic parameters now have the ability to characterize the macroscopic and microscopic mechanical properties of Jinping marble.

The test results of seven acoustic detection cross-sections arranged in Type II surrounding rock of 1# and 3# diversion tunnels were statistically averaged (Table 2). The test results of seven acoustic detection cross-sections arranged in Type III surrounding rock of 1# and 3# diversion tunnels were statistically averaged (Table 3).

Table 2. Statistics table of Sonic detection results of Type II surrounding rock cross sections in 1#, 3# diversion tunnels (Unit:m).

Detection Pile No.	Depth	Strata Lithology	Rock Type	North Wall	North Arch Shoulder	Top Arch	South Arch Shoulder	South Wall	Remark
(1#)14+750	1536	T_{2y}^{5}	II	1.4	2.6	1.2	2.0	2.2	/
(1#)14+280	1694	T_{2y}^{6}	II	1.6	1.2	1.8	1.4	1.6	1.6
(1#)12+970	1644	T_{2y}^{5}	II	1.2	1.2	1.2	1.0	0.8	/
(3#)15+850	935	T_{2y}^{6}	II	2.0	1.4	2.4	1.2	1.4	/
(3#)15+740	1028	T_{2y}^{5}	IIb	1.0	1.6	2.4	1.8	1.0	/
(3#)15+250	1293	T_{2y}^{5}	II	1.8	1.8	1.8	1.0	2.0	/
(3#)12+850	1724	T_{2y}^{5}	II	1.4	1.8	1.6	2.4	1.2	/
Average	1408			1.5	1.7	1.8	1.5	1.5	/

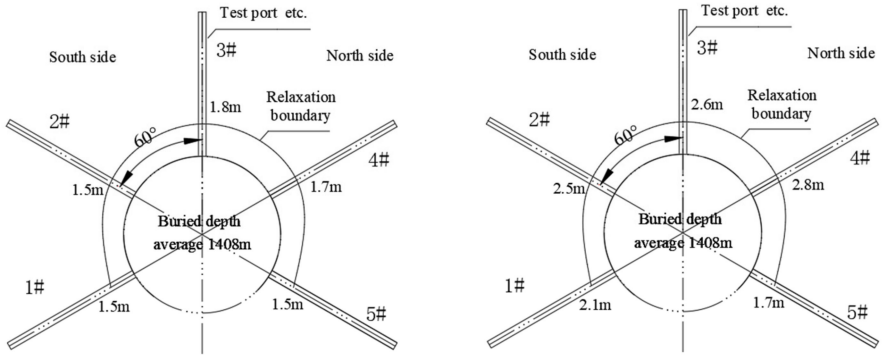
Table 3. Statistics table of sonic detection results of Type III surrounding rock cross sections in 1#, 3# diversion tunnels (Unit:m).

Detection Pile No.	Depth	Strata Lithology	Rock Type	North Wall	North Arch Shoulder	Top Arch	south Arch Shoulder	South Wall	Remark
(1#)14+955	1517	T_{2y}^{5}	III	1.4	2.0	2.6	1.6	3.6	/
(3#)15+200	1319	T_{2y}^{5}	III	1.0	3.4	3.4	3.2	1.2	/
(1#)15+150	1427	T_{2y}^{4}	III	2.6	2.8	2.2	1.2	1.4	/
(3#)14+975	1418	T_{2y}^{5}	III	2.0	3.2	2.6	3.8	2.8	/
(3#)14+920	1430	T_{2y}^{5}	III	1.0	3.2	2.4	2.2	1.2	/
(3#)14+635	1573	T_{2y}^{5}	III	1.4	2.6	2.6	3.0	3.4	/
(3#)14+505	1636	T_{2y}^{5}	III	2.6	2.6	2.4	2.2	1.4	/
Average	1474			1.7	2.8	2.6	2.5	2.1	

It can be known that in the acoustic detection cross-sections in Type II surrounding rock of 1# and 3# diversion tunnels, the average depths of the low-wave velocity zones in five parts, i.e., the north wall, the north arch shoulder, the top arch, the south arch shoulder, and the south wall are 1.5 m, 1.7 m, 1.8 m, 1.5 m, and 1.5 m, respectively. The maximum buried depth of the seven acoustic detection cross-sections is 1724 m; the minimum is 935 m, and the average is 1408 m. In the acoustic detection cross-sections in Type III surrounding rock of Jinping 1# and 3# diversion tunnels, the average depths of the low-wave velocity zone in five parts, i.e., the north wall, the north arch shoulder, the top arch, the south arch shoulder, and the south wall are 1.7 m, 2.8 m, 2.6 m, 2.5 m, and 2.1 m, respectively. The maximum buried depth of the seven acoustic detection cross-sections is 1636 m; the minimum is 1319 m, and the average is 1474 m.

Based on the above statistical results, the average relaxation depths of surrounding rock in Types II/III surrounding rock acoustic detection cross-sections of Jinping 1# and 3# diversion tunnels are illustrated in Figure 5.

A group of microscopic mechanical parameters obtained after hundreds of parameter tests are listed in Table 4 based on the calibration method for microscopic parameters of the model mentioned before, with reference to the ground stress field characteristics of Jinping deeply buried tunnels by Itasca Company, and the PFC method was used to describe the mechanical characteristics of Jinping Type II marble [37].



Detection hole No.	1#	2#	3#	4#	5#
Relaxation depth (m)	1.5	1.5	1.8	1.7	1.5

Detection hole No.	1#	2#	3#	4#	5#
Relaxation depth (m)	2.1	2.5	2.6	2.8	1.7

Figure 5. Statistical average relaxation depth of sonic detection sections with Type II/III surrounding rock in Jinping 1#, 3# diversion tunnel.

Table 4. Micro parameters of clumped-particle model for Jinping Type II/III marble.

Micro Parameters		Material Properties	
		Type II	**Type III**
Minimum particle size	$R_{\min}$ (m)	0.40	0.40
Particle size ratio	$R_{\max}/R_{\min}$	1.40	1.40
bulk density	ρ_ρ (kg/m^3)	2700	2700
Grain modulus	E_c (Gpa)	30.0	25.0
Particle stiffness ratio	k_n/k_s	2.5	1.5
Friction factor	μ	0.62	0.62
Contact bond tensile strength	σ_c (MPa)	24.0 ± 4.8	19.0 ± 3.8
Shear strength of contact bond	τ_c (MPa)	60.0 ± 12.0	57.0 ± 11.4
Tensile strength of parallel bond	$\overline{\sigma}_c$ (MPa)	18.0 ± 3.6	20.0 ± 4.0
Shear strength of parallel bond	$\overline{\tau}_c$ (MPa)	45.0 ± 9.0	60.0 ± 12.0
Parallel bond modulus	$\overline{E}_c$ (GPa)	30.0	25.0
Parallel bond stiffness ratio	$\overline{k}_n/\overline{k}_s$	2.5	2.5
Parallel bond radius factor	$\overline{\lambda}$	1.0	1.0
Morphological characteristics of cluster elements	clp_rad	L:R:r = 2.1:1.0:0.5	L:R:r = 2.1:1.0:0.5

In Table 4, the morphological characteristics and related geometric dimensions of cluster units for the replacement of the round particles in the BPM model are shown in Figure 6. It should be noted that some contacts unbonded are reserved in the CPM model medium in the parameter verification process to reflect the initial defect state of natural rock materials.

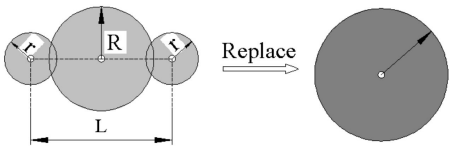


Figure 6. Morphological characteristics of clump element.

The compression test results of Jinping Type II marble model specimens described by the microscopic parameters in Table 4 under different confining pressures are shown in Figure 7. The left diagram in Figure 7 is the stress–strain curves of the model specimens under different confining pressures, and the right diagram in Figure 7 is the fitting results of the peak strength and the Hoek–Brown failure criterion of the model specimens under

different confining pressures. It can be seen that the PFC numerical test results display brittle characteristics of the model medium under low confining pressure (such as 1 MPa). When the confining pressure rises to about 10 MPa, the model medium is of obvious ductile characteristics. When the confining pressure jumps to about 15 MPa, the model medium presents obvious plastic characteristics. The above test results of model specimens suggest that the brittle-ductile-plastic transformation characteristics of Jinping Type II marble are reasonably described by the microscopic parameters shown in Table 4.

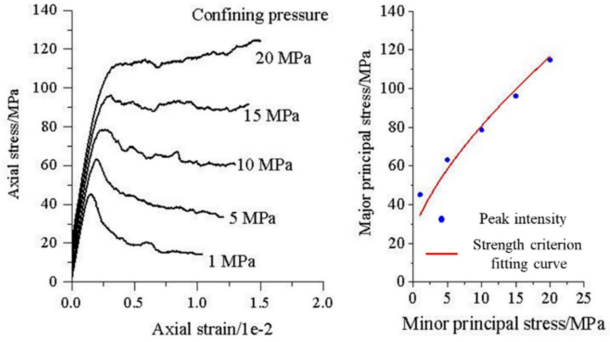


Figure 7. PFC test results of mechanical properties of model media for Jinping Type II marble.

The on-site rationality of "numerical material" was verified by adopting the "generalized" acoustic detection results of Type II marble. Figure 8 is the calculation results of excavation damage depth of Type II marble cross-sections under the condition of 1408 m depth based on the microscopic parameters of CPM model.

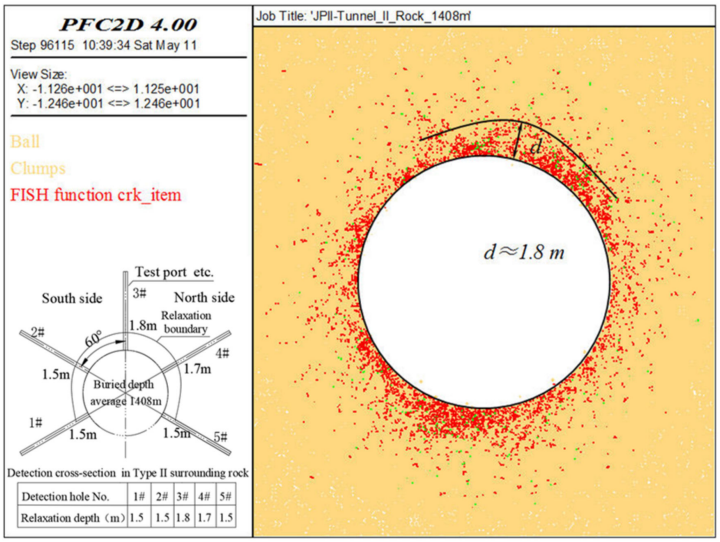


Figure 8. Excavation damage distribution of Type II marble under buried depth of 1408 m.

It can be seen from Figure 8 that after tunnel excavation, the micro-cracks are more developed in the north arch shoulder and top arch and the south arch foot, and the depth of zone with relatively developed cracks is about 1.8 m, which is basically consistent with the depth of the low-wave velocity zone at the north arch shoulder of the target cross-section shown in Figure 8.

Similar to the PFC microscopic parameters calibration method of Type II marble, the PFC microscopic parameters of Jinping Type III marble are also given in Table 4. It should be noted that CPM particles account for 80% and standard circular particles account for 20% in the model medium. In addition, some contacts unbonded are reserved in the model medium to reflect the initial defect characteristics of natural rock materials.

The compression test results of Jinping Type III marble model specimens under different confining pressures described by the microscopic parameters in Table 4 are shown in Figure 9. The left diagram in Figure 9 is the stress–strain curve of the model specimens under different confining pressures, and the right diagram in Figure 9 is the fitting results of the peak strength and the Hoek–Brown failure criterion of the model specimens under different confining pressures. The test results also reveal the brittle characteristics of Type III marble model medium at a low confining pressure. When the confining pressure increases to about 6 MPa, the model specimen displays certain ductile characteristics. When the confining pressure continues to rise to about 12 MPa, the model specimen shows obvious plastic properties. It can be seen that the brittle-ductile and ductile-plastic transformation confining pressures of Jinping Type III marble is slightly smaller than that of Jinping Type II marble, and its brittle-ductile-plastic transformation characteristics are reasonably described by the microscopic parameters shown in Table 4.

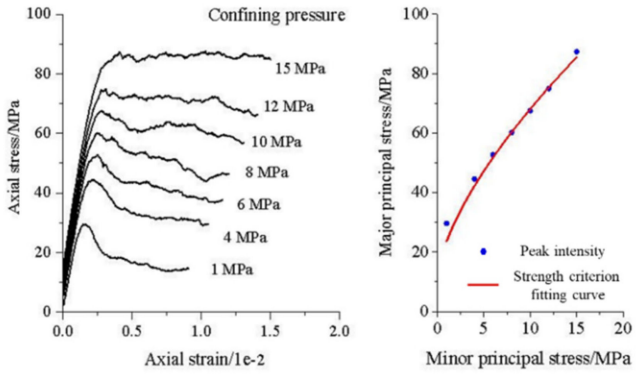


Figure 9. PFC test results of mechanical properties of model media for Jinping Type III marble.

Similar to the on-site verification method of Jinping Type II marble PFC model medium, the on-site rationality of Jinping Type III marble PFC model medium was also verified by adopting the acoustic detection results of Type III marble after "generalization". Figure 10 shows the calculation results of excavation damage depth of Type III marble cross-section under the condition of 1474 m depth through the above PFC model microscopic parameters. Due to the decrease in rock quality, the damage depth and micro-crack development density of surrounding rock after tunnel excavation increase remarkably. That is, the depth and degree of surrounding rock excavation damage rise. Overall, the damage cracks are developed in the north arch shoulder and top arch, and the south arch foot. The depth of the zone with relatively developed cracks is about 2.8 m, which is basically consistent with the depth of the low-wave velocity zone at the north arch shoulder of the target cross-section in Figure 10.

The above numerical test results show that the PFC model medium material of Jinping Types II/III marble shown in Table 4 can meet the description of Types II/III marble by the Hoek–Brown failure criterion and the acoustic detection results of the relaxation depth of surrounding rock on site. Moreover, the model specimen can naturally reflect the brittle-ductile-plastic transformation characteristics with the increase in confining pressure. Therefore, it can be considered that the PFC microscopic parameters have the ability to characterize the macroscopic and microscopic mechanical characteristics of Jinping Types II/III marble, and the results well disclose the excavation damage characteristics of deeply buried tunnel surrounding rock. It can also provide a reasonable basis for the prediction of the fracturing damage characteristics of surrounding rock under TBM excavation under the conditions of Types II/III rock mass in deeply buried marble tunnel sections.

It should be noted that, in view of the randomness of joint fissure distribution and the influence of other factors, the quality of rock mass on site varies greatly. Even if the same Class III wall rock section is buried at a similar depth, the distribution characteristics of the low wave velocity zone on the section may be significantly different, which can be

seen from Tables 2 and 3. This is why the acoustic testing results of the relaxation depth of the surrounding rock on site should be homogenized as the on-site basis for parameter verification. This treatment is equivalent to that the uniaxial compressive strength of rock is not the test result of a certain specimen, but the average value of the test results of many specimens. Accordingly, Figures 8 and 10 are the comparison results of the meso parameters of Class II/III marble and the acoustic monitoring section after field homogenization, which are equivalent to the field verification. The results show that the meso parameters of Class II/III marble in Table 4 can reasonably describe the physical and mechanical properties of Class II/III marble, and are consistent with the field test results of the low wave velocity zone of the tunnel surrounding rock after excavation, which can be used to simulate the damage characteristics of the surrounding rock in the deep tunnel section of TBM excavation.

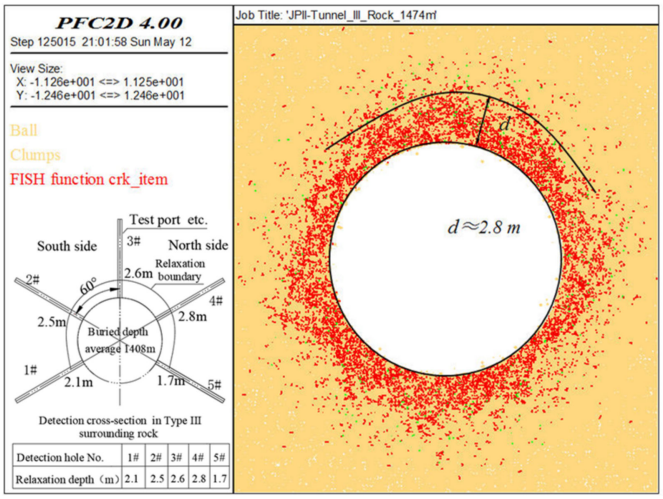


Figure 10. Excavation damage distribution of Type III marble under buried depth of 1474 m.

5. Excavation Damage Characteristics of Surrounding Rock in Deeply Buried Tunnel Sections

The verification and field verification of the microscopic parameters of Jinping II/III marble CPM model show that that the PFC model medium material in Table 4 can reasonably describe the physical and mechanical properties of Types II/III marble, and are consistent with the on-site test results of the low-wave velocity zone of the tunnel surrounding rock after excavation. This lays a solid foundation for the simulation study of surrounding rock excavation damage characteristics of the TBM excavation of Jinping deeply buried marble tunnel sections.

The prediction of surrounding rock damage depth of TBM excavation in Jinping deep marble tunnel sections basically coincides with the calculation process of on-site verification of PFC model parameters. The difference is that the initial on-site stress needs to be adjusted according to the variation of buried depth. Figures 11 and 12 are the distribution characteristics of surrounding rock excavation damage in TBM excavation of Types II/III marble tunnels respectively under the conditions of 1750 m, 1900 m, 2000 m, 2100 m, 2200 m, 2300 m, 2400 m, and 2500 m. Overall, the EDZs of surrounding rock of Types II/III marble sections are unevenly distributed around Jinping tunnels, and the largest EDZ is from the top arch to the north arch shoulder. With the increase in buried depth, the depth and degree of surrounding rock excavation damage rise, and the increase in damage degree is mainly illustrated by the increase in crack density.

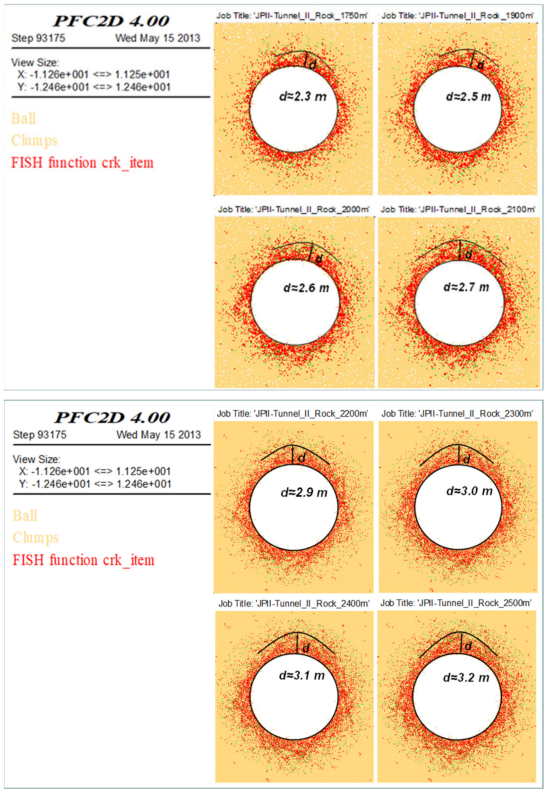


Figure 11. Excavation damage feature of Jinping Type II Marble excavated by TBM under 1750 m ~ 2500 m.

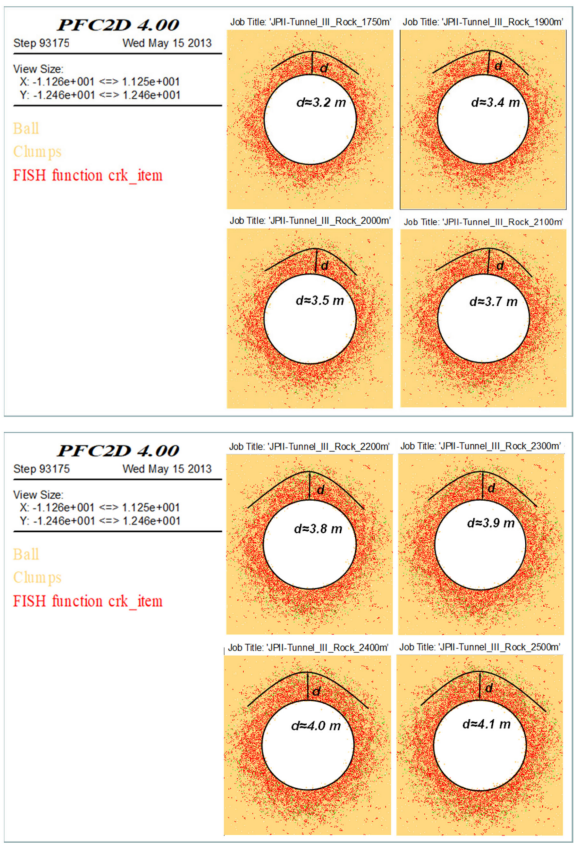


Figure 12. Excavation damage feature of Jinping Type III Marble excavated by TBM under 1750 m ~ 2500 m.

According to the calculation results, the statistical results of the maximum excavation damage depth of surrounding rock under TBM excavation condition in Jinping deeply buried tunnel sections are given in Table 5.

Table 5. The predicted maximum depth of the excavation damage zone of Jinping tunnels.

Buried Depth (m)	The Maximum Depth of EDZ of Surrounding Rock (m)	
	Type II	Type III
1750	2.3	3.2
1900	2.5	3.4
2000	2.6	3.5
2100	2.7	3.7
2200	2.9	3.8
2300	3.0	3.9
2400	3.1	4.0
2500	3.2	4.1

The above prediction results suggest that under the same buried depth condition, with the decrease in rock quality, the EDZ depth and damage degree of surrounding rock rise. Overall, the maximum damage depth of Jinping Type III surrounding rock is about 1.0 m larger than that of Type II surrounding rock, which is basically consistent with the acoustic detection results obtained on site.

It should be noted that the above statistical results of excavation damage depth of surrounding rock were directly measured based on the calculation. Theoretically, this method may not be accurate enough, but in terms of engineering application, the error is acceptable.

6. Conclusions

In view of the excavation damage characteristics of tunnel surrounding rock of Jinping deeply buried marble, the PFC microscopic parameters of Types II/III marble tunnels were simulated and calibrated with the aid of PFC^{2D} program according to the acoustic detection results of tunnel cross-sections under the condition of TBM obtained on site. Therefore, the excavation damage characteristics of surrounding rock of deeply buried sections in Jinping diversion tunnels were simulated. The main conclusions obtained are as follows:

(1) From the perspective of rationality of the damage research method, CMM has inevitable defects in describing some mechanical problems of rock mass. For example, it is not applicable to describing the discontinuous mechanical problems of rock mass. Instead, indirect methods have to be adopted to deal with some complex mechanical behaviors caused by the fracturing of surrounding rock. Therefore, the DMM-based PFC program is obviously superior in the study on excavation damage problem of Jinping deeply buried tunnels.

(2) In the acoustic detection results of the relaxation depth of the tunnel cross-sections, even the detection results of different test holes in the same cross-section may differ much for the following reasons: the influence of the difference in rock quality between cross-sections, structural plane, and local stress field and the large dispersion of the relaxation depth of the cross-sections. Therefore, acoustic detection results of the relaxation depth should be "generalized": the structural plane in the rock mass is homogenized. That is, when the influence of the structural plane is reflected in the integrity index of the rock mass, the "homogenized" calculation results of the model should be consistent with the on-site test results under "general conditions".

(3) Based on the "generalized" analysis on the acoustic detection results of tunnel cross-sections under the condition of TBM excavation, the PFC microscopic parameters of Jinping Types II/III marble were simulated and calibrated. The results disclose that the obtained PFC model material of Jinping Types II/III marble conforms to not only the

description of Jinping Types II/III marble in deeply buried tunnels by the Hoek–Brown failure criterion, but also the acoustic test results of the relaxation depth of surrounding rock under "general conditions". Meanwhile, the model specimen can naturally reflect the brittle-ductile-plastic transformation characteristics with the increase in confining pressure.

(4) The EDZs of surrounding rock of Types II/III marble sections in Jinping tunnels are unevenly distributed around the tunnels, with the largest EDZ being from the top arch to the north arch shoulder. With the increase in buried depth, the EDZ depth and damage degree of surrounding rock increase. With the decrease in rock quality, the EDZ depth and damage degree of surrounding rock increase. Overall, the maximum damage depth of Type III surrounding rock is about 1.0 m larger than that of Type II surrounding rock under the same buried depth, which is basically consistent with the detection results of the relaxation depth of surrounding rock. The simulation well discloses surrounding rock excavation damage characteristics of Jinping deeply buried tunnels.

The methods and contents in this research can provide reference for the study on excavation damage of rock mass and its evolution mechanism as well as for surrounding rock stability analysis and support optimization design of deeply buried rock mass engineering.

The actual site conditions include the influence of fissure water, which has not been carried out in the software for the time being. Due to the efficiency of the software calculation, this study only uses the two-dimensional PFC model, and the subsequent consideration is to use the three-dimensional PFC model to further study such problems.

Author Contributions: Conceptualization, Y.Z. (Yanbin Zhang); validation, Y.Z. (Yongsheng Zhu); formal analysis, H.Y. and Y.Z. (Yongsheng Zhu); investigation, H.Y.; resources, H.Y.; data curation, Y.Z. (Yanbin Zhang); writing—original draft, H.Z.; writing—review and editing, H.Z.; visualization, Y.Z. (Yongsheng Zhu); supervision, Y.Z. (Yanbin Zhang); project administration, H.Z.; funding acquisition, Y.Z. (Yanbin Zhang). All authors have read and agreed to the published version of the manuscript.

Funding: This work was funded by National Natural Science Foundation of China (U1810203), Doctoral Program of Henan Polytechnic University (No.B2015-53).

Acknowledgments: This work was supported by National Natural Science Foundation of China (U1810203), Doctoral Program of Henan Polytechnic University (No.B2015-53). During the research and writing of the thesis, Zhu Huanchun from Itasca China gave strong support and assistance to the diversion tunnel project of Jinping II Hydropower Station, and provided PFC2D software for the research of this paper for free. I would like to express my sincere thanks.

Conflicts of Interest: The authors declare that they have no known competing financial interests or personal relationships that could have appeared to influence the work reported in this paper.

References

1. Guo, H.; Tong, J.; Sun, Q.; Xu, Y.; Luo, W. Determination method of excavation damage zone based on surrounding rock damage-fracture ratio in underground engineering. *Front. Earth Sci.* **2022**, *357*, 836313. [CrossRef]
2. Backblom, G.; Martin, C.D. Recent experiments in hard rocks to study the excavation response: Implications for the performance of a nuclear waste geological repository. *Tunn. Undergr. Space Technol.* **1999**, *14*, 377–394. [CrossRef]
3. Read, R.S. 20 years of excavation response studies at AECL's Underground Research Laboratory. *Int. J. Rock Mech. Min.* **2004**, *41*, 1251–1275. [CrossRef]
4. Yang, C.; Hu, Z.; Huang, D.; Guo, F. Failure mechanism of primary support for a shallow and asymmetrically loaded tunnel portal and treatment measures. *J. Perform. Constr. Fac.* **2020**, *34*, 4019105. [CrossRef]
5. Xie, L.; Yan, P.; Lu, W.; Chen, M.; Wang, G. Effects of strain energy adjustment: A case study of rock failure modes during deep tunnel excavation with different methods. *Ksce J. Civ. Eng.* **2018**, *22*, 4143–4154. [CrossRef]
6. Tang, B.; Cheng, H.; Tang, Y.; Zheng, T.; Yao, Z.; Wang, C.; Rong, C. Supporting design optimization of tunnel boring machines-excavated coal mine roadways: A case study in Zhangji, China. *Processes* **2020**, *8*, 46. [CrossRef]
7. Chen, S.; Feng, F.; Wang, Y.; Li, D.; Huang, W.; Zhao, X.; Jiang, N. Tunnel failure in hard rock with multiple weak planes due to excavation unloading of in-situ stress. *J. Cent. South Univ.* **2020**, *27*, 2864–2882. [CrossRef]
8. Potyondy, D.O.; Cundall, P.A. Modeling notch-formation mechanisms in the URL mine-by test tunnel using bonded assemblies of circular particles. *Int. J. Rock Mech. Min.* **1998**, *4*, 510–511. [CrossRef]
9. Martin, C.D.; Simmons, G.R. The Underground Research Laboratory: An opportunity for basic rock mechanics. *ISRM News J.* **1992**, *1*, 4–12.

10. Carlson, S.R.; Young, R.P. *Acoustic Emission and Ultrasonic Velocity Study of Excavation-Induced Microcrack Damage at the Underground Research Laboratory*; Elsevier: Amsterdam, The Netherlands, 1993; pp. 901–907.
11. Fairhurst, C. Nuclear waste disposal and rock mechanics: Contributions of the Underground Research Laboratory (URL), Pinawa, Manitoba, Canada. *Int. J. Rock Mech. Min.* **2004**, *41*, 1221–1227. [CrossRef]
12. Stanfors, R.; Rhén, I.; Tullborg, E.; Wikberg, P. Overview of geological and hydrogeological conditions of the Aspö hard rock laboratory site. *Appl. Geochem.* **1999**, *14*, 819–834. [CrossRef]
13. Hsiung, S.M.; Chowdhury, A.H.; Nataraja, M.S. Numerical simulation of thermal–mechanical processes observed at the Drift-Scale Heater Test at Yucca Mountain, Nevada, USA. *Int. J. Rock Mech. Min.* **2005**, *42*, 652–666. [CrossRef]
14. Ma, J.; Yin, P.; Huang, L.; Liang, Y. The application of distinct lattice spring model to zonal disintegration within deep rock masses. *Tunn. Undergr. Space Technol.* **2019**, *90*, 144–161. [CrossRef]
15. Ma, J.; Chen, J.; Chen, W.; Huang, L. A coupled thermal-elastic-plastic-damage model for concrete subjected to dynamic loading. *Int. J. Plast.* **2022**, *153*, 103279. [CrossRef]
16. Ma, J.; Zhao, G.; Khalili, N. An elastoplastic damage model for fractured porous media. *Mech Mater* **2016**, *100*, 41–54. [CrossRef]
17. Yan, P.; Lu, W.B.; Chen, M.; Shan, Z.G.; Chen, X.R. In-situ test research on influence of excavation method on induced damage zone in deep tunnel. *Chin. J. Rock Mech. Eng.* **2011**, *30*, 1097–1106.
18. Zhu, Z.Q.; Sheng, Q.; Zhang, Y.; Li, Y. Research on excavation damage zone of underground powerhouse of Dagangshan hydropower station. *Chin. J. Rock Mech. Eng.* **2013**, *32*, 734–739.
19. Liu, N.; Zhang, C.; Chu, W. Depth of fracture and damage in deep-buried surrounding rock and bolt length design. *Chin. J. Rock Mech. Eng.* **2015**, *34*, 2278–2284.
20. Wu, Z.; Jiang, Y.; Liu, Q.; Ma, H. Investigation of the excavation damaged zone around deep TBM tunnel using a Voronoi-element based explicit numerical manifold method. *Int. J. Rock Mech. Min.* **2018**, *112*, 158–170. [CrossRef]
21. Yang, J.; Yang, X.; Zhou, J.; Liu, Y.; Dong, B.; Li, H. Comparative study of the excavation damage and rockburst of the deeply buried jinping II diversion tunnels using a TBM and the drilling-blasting method. *Adv. Civ. Eng.* **2020**, *2020*. [CrossRef]
22. Hu, M.; Zhou, H.; Zhang, Y.; Zhang, C.; Gao, Y.; Hu, D.; Lu, J. Acoustic emission monitoring on damage evolution of surrounding rock during headrace tunnel excavation by TBM. *Eur. J. Environ. Civ. Eng.* **2019**, *23*, 1248–1264. [CrossRef]
23. Cho, N.; Martin, C.D.; Sego, D.C. Development of a shear zone in brittle rock subjected to direct shear. *Int. J. Rock Mech. Min.* **2008**, *45*, 1335–1346. [CrossRef]
24. Nasehi, S.A.; Uromeihy, A.; Nikudel, M.R.; Morsali, A. Influence of gas oil contamination on geotechnical properties of fine and coarse-grained soils. *Geotech. Geol. Eng.* **2016**, *34*, 333–345. [CrossRef]
25. Khuntia, S.; Mujtaba, H.; Patra, C.; Farooq, K.; Sivakugan, N.; Das, B.M. Prediction of compaction parameters of coarse grained soil using multivariate adaptive regression splines (MARS). *Int. J. Geotech. Eng.* **2015**, *9*, 79–88. [CrossRef]
26. Ivars, D.M.; Pierce, M.E.; Darcel, C.; Reyes-Montes, J.; Potyondy, D.O.; Young, R.P.; Cundall, P.A. The synthetic rock mass approach for jointed rock mass modelling. *Int. J. Rock Mech. Min.* **2011**, *48*, 219–244. [CrossRef]
27. Zhu, H.C.; Wu, J.Y.; Zhu, Y.S.; Yu, H.Z.; Chu, W.J.; Meng, G.T.; Huang, D.; Li, H.; Andrew, C.; Loren, L.; et al. *Research on Surrounding Rock Stability, Dynamic Supporting Design of Jinping II Hydropower Station Diversion Tunnel—2010 Stage Summary Report*; Itasca Consulting Co., Ltd.: Wuhan, China, 2010. (In Chinese)
28. Afolagboye, L.O.; He, J.; Wang, S. Experimental study on cracking behaviour of moulded gypsum containing two non-parallel overlapping flaws under uniaxial compression. *Acta Mech Sin.* **2017**, *33*, 394–405. [CrossRef]
29. Marot, D.; Bendahmane, F.; Le, V.T. *New Apparatus for Assessing Soil Suffusion Susceptibility under Two Flow Directions*; Springer: Berlin/Heidelberg, Germany, 2018; pp. 69–80.
30. Li, H.; Ma, H.; Shi, X.; Zhou, J.; Zhang, H.; Daemen, J. A 3D grain-based model for simulating the micromechanical behavior of salt rock. *Rock Mech. Rock Eng.* **2020**, *53*, 2819–2837. [CrossRef]
31. Marot, D.; Rochim, A.; Nguyen, H.; Bendahmane, F.; Sibille, L. Assessing the susceptibility of gap-graded soils to internal erosion: Proposition of a new experimental methodology. *Nat. Hazards* **2016**, *83*, 365–388. [CrossRef]
32. Pachideh, V.; Hosseini, S.M.M.M. A new physical model for studying flow direction and other influencing parameters on the internal erosion of soils. *Geotech. Test. J.* **2018**, *42*, 1431–1456. [CrossRef]
33. Zhang, C.S.; Chen, X.R.; Hou, J.; Chu, W.J. Study of mechanical behavior of deep-buried marble at Jinping II hydropower station. *Chin. J. Rock Mech. Eng.* **2010**, *29*, 1999–2009.
34. Wawersik, W.R.; Fairhurst, C.H. *A Study of Brittle Rock Fracture in Laboratory Compression Experiments*; Elsevier: Amsterdam, The Netherlands, 1970; pp. 561–575.
35. Yu, H.A.; Ruan, H.N.; Chu, W.J. PFC modeling of brittle- ductile-plastic transition character of marble. *Chin. J. Rock Mech. Eng.* **2013**, *32*, 55–64. (In Chinese) [CrossRef]
36. You, M.Q. *Strength of Rock Specimen and Its Deformation and Failure Process*; Geological Publishing House: Beijing, China, 2000; pp. 86–112. (In Chinese)
37. Itasca Consulting Group. *PFC2D (Particle Flow Code in 2 Dimensions) User's Guide*; Itasca Consulting Group: Minneapolis, MN, USA, 2008; Volume 42.